ISSN 0027-1349, Moscow University Physics Bulletin, 2015, Vol. 70, No. 6, pp. 541–548. © Allerton Press, Inc., 2015.
Original Russian Text © V.E. Kunitsyn, B.Yu. Krysanov, A.M. Vorontsov, 2015, published in Vestnik Moskovskogo Universiteta. Fizika, 2015, No. 6, pp. 112–119.

PHYSICS OF EARTH, ATMOSPHERE, AND HYDROSPHERE

Acoustic-Gravity Waves in the Earth's Atmosphere Generated by Surface Sources

V. E. Kunitsyn, B. Yu. Krysanov, and A. M. Vorontsov

Department of Physics, Moscow State University, Moscow, 119991 Russia

e-mail: am.vorontsov@physics.msu.ru

Received June 8, 2015; in final form, July 29, 2015

Abstract—The generation of acoustic-gravity waves and their propagation in the Earth's atmosphere is analyzed numerically on the basis of a computer model of the stratified atmosphere with dissipation. Atmospheric and ionospheric wavelike disturbances from different surface sources such as earthquakes, explosions, seiches, temperature heating, and tsunamis are studied.

Keywords: ionosphere, acoustic-gravity waves, Earth's surface perturbations, Euler's equations.

DOI: 10.3103/S0027134915060120

INTRODUCTION

The Earth's atmosphere and ionosphere are sensitive indicators of different natural and anthropogenic disturbances of the Earth's surface or Ocean. Natural disturbance sources include earthquakes, tsunamis, geomagnetic activity, seiches, and so on, and artificial sources include different chemical and nuclear explosions, and space-vehicle launches. Disturbances from these sources propagate into the atmosphere with acoustic-gravity waves (AGWs). The Earth's atmosphere density sharply decreases with altitude; therefore, AGWs amplify during their propagation upward and significantly disturb the upper atmosphere and ionosphere. Thus, the wave amplification factor attains four orders of magnitude for some surface sources at ionospheric altitudes [1]. These ionospheric disturbances are recorded in large spatial regions with the use of modern techniques for the study of the upper atmosphere, such as satellite radio tomography or incoherent radio scattering.

Disturbances in the upper atmosphere, which occur several hours or even days before a strong earthquake, are currently actively studied [2]. According to the hypothesis [3], AGW generation is induced by prefault processes in the region of earthquake preparation near the Earth's surface; they propagate to ionospheric altitudes and form ionospheric precursors of the earthquake [4].

This example shows that the study of different ionospheric events provides representation of current or expected surface or space disturbances under conditions of correct interpretation of the events and an understanding of how they form. The question about the transfer of acoustic energy from surface sources to circumterrestrial space is the least understood, due to the insufficient development of the theory of AGW propagation in the real atmosphere. In addition, reliable data on the main parameters of ionospheric responses to surface disturbances (amplitude, profile, period, phase and group travel velocities of wave packet) and angular parameters of the wave vector should be known for the comprehensive analysis. We should note the wide spreads in the literature data on the key parameters of AGWs that are excited by different surface disturbances and ideas about how AGWs are generated. The ideas that have been suggested are: generation of infrasonic waves [1], generation of internal gravity waves [5], vortex motions of the neutral atmospheric component induced after passage of an acoustic pulse [6], generation of acoustic-shock waves [7], and so on.

Thus, the problem of the simulation of the responses of the upper atmosphere to disturbances from different sources (underground, surface, or near-surface) is becoming urgent. It allows assessment of the key parameters of these responses and realization of how they are formed. The aim of this work is the numerical simulation of AGW generation and propagation in a 2D compressible dissipative nonlinear atmosphere for different classes of surface sources, analysis of the results, and determination of the regularities in AGW propagation.

1. STATEMENT OF THE PROBLEM AND A NUMERICAL MODEL FOR ITS SOLUTION

The basic set of equations for the analysis of AGW generation and propagation is the set of Euler's geo-

physical hydrodynamic equations [8], which considers the atmospheric stratification, zonal wind, dissipative effects, and nonlinearity:

$$\begin{gathered}\frac{\partial \rho}{\partial t} + \nabla(\rho v) = 0,\\ \rho\left(\frac{\partial v}{\partial t} + (v,\nabla)v\right) = -\nabla p + \rho \mathbf{g} + \mathbf{F}_d,\\ \rho\left(\frac{\partial (c_v T)}{\partial t} + (v,\nabla)(c_v T)\right) = -p(\nabla, v) + Q_d,\\ p = \frac{\rho}{m_0} RT.\end{gathered} \quad (1)$$

The first equation is the continuity equation, the second one is the momentum equation (Navier–Stokes), the third one is the energy-conservation equation, and the fourth equation is the ideal gas law. The Coriolis force is negligible for such rapid motions and, hence, is ignored in this case. Here ρ is the density, T is the temperature, p is the pressure, v is the medium particle velocity in the wave, $\mathbf{g}$ is the gravity acceleration, $\mathbf{F}_d$ is the viscosity force, Q_d is the heat absorbed due to the wave dissipation, c_v is the gas specific capacity at a constant volume, m_0 is the relative molecular mass of air, R is the universal gas constant, $\nabla = \partial/\partial \mathbf{r}$, and r is the spatial coordinate.

The Navier–Stokes equation is the basis of geophysical hydrodynamic equations (1); it is applicable to the atmosphere up to altitudes of 500–600 km. The atmospheric disturbances under study are usually recorded up to these altitudes; hence, this equation can be used for the solution of the stated problems.

Internal gravity waves (IGWs) are of the highest intensity in the AGW spectrum. IGWs dissipate in the upper atmosphere due to, first of all, molecular viscosity, thermal conduction, and ion deceleration. Considering these causes, the force, $\mathbf{F}_d$, was taken in the Rayleigh form: $\mathbf{F}_d = -\alpha v$. Here α is the coefficient of resistance; its values at different altitudes correspond to different dissipation mechanisms. There are no data on the values and altitude variations in the coefficient α in the literature. Moreover, which causes at which altitudes predominate in AGW dissipation are still unknown. In [9], $\chi = \alpha/\rho$ was assumed to be constant, and the coefficient χ was chosen from tests of the model at different values of this parameter. In addition, dissipation due to the above causes requires several days to damp the energy of such large-scale wave motions [10]; therefore, the dissipative term in the temperature equation can be set equal to zero: $Q_d = 0$.

To integrate set (1) numerically, it is convenient to divide the density, pressure, and temperature into two parts (time-independent and disturbed) and rewrite the set in terms of these disturbances. In addition, the resulting set is to be reduced to a dimensionless form. The final set of equation that are suitable for numerical integration is given, e.g., in [9].

Let us consider the resulting set of equation in the 2D geometry and find its solution in a certain rectangular domain; the Earth's radius curvature is assumed to have no effect on the results. Let us introduce the Cartesian coordinates Oxz so as the Oz axis is directed vertically upward and the Ox axis is directed horizontally. In these coordinates, $\mathbf{r} = (x, z)$ and $v = (u, w)$, where u (w) is the horizontal (vertical) component of the medium particle velocity.

To solve the set of equations, the initial and boundary conditions should be specified. The initial conditions for the velocity and disturbances of density, pressure, and temperature are chosen zero. For the boundary condition at the bottom boundary of the simulation domain, a parameter (velocity or temperature) in the surface air layer is set to be equal to the corresponding value on the Earth's surface. This boundary condition ensures the disturbance transfer from a surface source into the atmosphere. Other variables are considered to be continuous during passage through the surface of the bottom boundary. Ordinary boundary conditions were applied to the upper and side boundaries to ensure wave propagation through these walls without noticeable reflection. The flux correct transport (FCT) method of the second-order accuracy in time and spatial variables was used for the numerical calculation [11].

2. MODELS OF SURFACE SOURCES OF DISTURBANCES

Atmospheric disturbances from surface sources of different nature are studied numerically in this work; the mathematical models of the sources are described below. Each source is specified as a disturbance of the Earth–atmosphere interface, has a unique set of parameters to characterized it, and simulates a real natural or anthropogenic source that is capable of generating AGWs in the upper atmosphere.

Let us consider a source that simulates short- and long-period oscillations of the Earth's surface typical for underground explosions and shallow earthquakes in the first case and seismogravitational oscillations in the second case. Again, a vertical displacement of the Earth's surface $h(x, z = 0, t)$ is representable to a certain approximation as a local function $f(x)$ that specifies the pulse shape and is, in the simplest case, a product of a gaussoid and a periodic function that depends only on time and determines the time dynamics of the disturbance. The time derivation of this displacement determines the vertical motion velocity, w, of hydrodynamic particles of the Earth–atmosphere interface. Thus, to describe earthquakes, explosions, and long-period oscillations of the Earth's surface, the

following boundary conditions can be specified for the vertical velocity:

$$w(x, z = 0, t) = \frac{\partial h(x, z = 0, t)}{\partial t} = w_0 \cos\left(\frac{2\pi}{P}(t - t_0)\right) f(x), \quad t_0 \le t \le t_0 + nP,$$

remaining other thermodynamic parameters undisturbed at the bottom boundary of the simulation domain. Here w_0 characterizes the disturbance amplitude, t_0 is the time of disturbance onset, P is the oscillation period, and n is an integer hereinafter. The oscillation period P is quite small, on the order of fractions of second ($P < 1$ s), for earthquakes and explosions; vice versa, the oscillation amplitude w_0 is quite large, 1–100 m/s at the source center [6]. The period of possible oscillations is from 10 s to several hours for long-period oscillations of the Earth's surface and the oscillation amplitude, w_0, does not exceed 1 m/s [2, 4]. The spatial pulse width, $f(x)$, is characterized by the longitudinal scale of the disturbance, D_x; hence, in the case of a gaussian, $f(x) = \exp\left(-(x - x_c)^2/D_x^2\right)$ (x_c is the pulse-center coordinate).

Seiches are another important example of surface sources that are capable of inducing disturbances in the upper atmosphere. Seiches are long-period oscillations of the water surface which are induced in relatively enclosed water bodies, mainly by wind in a certain part of a lake or bay; they are water surface oscillations with amplitudes from several millimeters to several meters near coasts and periods from several minutes to several tens of hours [12]. Usually, the larger the area and spatial scales of an enclosed water body the longer the period is. Several oscillations modes are distinguished in the seiche composition; however, according to studies, most of the oscillation energy falls to the first mode.

Let us assume that the vertical displacement of the water body surface corresponding to the first seiche mode is representable as

$$h(x, z = 0, t) = h_0 f(t) \cos\left(\frac{\pi}{D_x}(x - x_c)\right), \quad t_0 \le t \le t_0 + nP, \quad |x - x_c| \le D_x,$$

where h_0 is the displacement amplitude, D_x is the characteristic longitudinal scale of the displacement, and the function $f(t)$, which determines the time dynamics of the disturbance, is representable as sine oscillations in the simplest case: $f(t) = \sin(2\pi(t - t_0)/P)$. The function h is discontinuous at the edges of the segment $|x - x_c| \le D_x$, which should be smoothed using, e.g., joining with third-order B-splines that provide for an equal-zero resulting function and its derivative at the points of a new boundary of the disturbance carrier.

One more important class of AGW generation sources includes temperature inversions in the lower atmosphere, volcanic eruptions, disturbance of an air stream by (warm) megalopolises, insolation, and photodissociation in the atmosphere [13]. All these phenomena have a common characteristic feature, viz., they are connected with local variations in the surface temperature. In addition, it is well known that temperature variations can occur near the Earth's surface during the compression phase of seismogravitational oscillations due to emissions of lithospheric gases into the atmosphere. This phenomenon was observed during meteorological measurements in Middle Asia several hours (sometimes days) before several strong earthquakes. Local increases in the temperature near foci of strong earthquakes were also recorded in satellite observations of the Earth's surface in earthquake regions [4] several days before the main shock.

Thus, the simulation of responses of the upper atmosphere to such temperature sources is also an urgent problem. The following temperature function was specified at the bottom boundary as a hypothetic source:

$$T(x, z = 0, t) = T_0 \sin^2\left(\frac{2\pi}{P}(t - t_0)\right) f(x), \quad t_0 \le t \le t_0 + nP,$$

where T_0 characterizes the disturbance amplitude in temperature units and $f(x)$ characterizes the pulse shape. The function $f(x)$ was taken in the form $f(x) = \exp\left(-(x - x_c)^2/D_x^2\right)$, so that this function approximately describes most of the above-mentioned temperature sources at $D_x = 20$–100 km. The periods of these phenomena are very different and can be roughly assessed by tens of minutes to tens of hours.

Tsunamis, as dangerous and strong natural phenomena, have been an object of study for a quite a long time. Numerous and varied materials have been collected on this subject matter [14]; they allow one to assert that a tsunami is among the strongest surface sources of disturbances in the upper atmosphere. In this work, we assume that a vertical displacement of the ocean surface that corresponds to tsunami propagation can be represented as

$$h(x, z = 0, t) = h_0 f(t) \exp(-(x - \nu t)^2/\lambda^2),$$

where h_0 is the tsunami height, ν is the horizontal propagation velocity, and λ is the spatial scale or length of a single wave. The function $f(t)$ is a time function that specifies the tsunami amplitude, or, in view of the constant wave propagation velocity in the model suggested, the amplitude of the vertical displacement of the water surface versus the longitudinal coordinate. This function describes the development

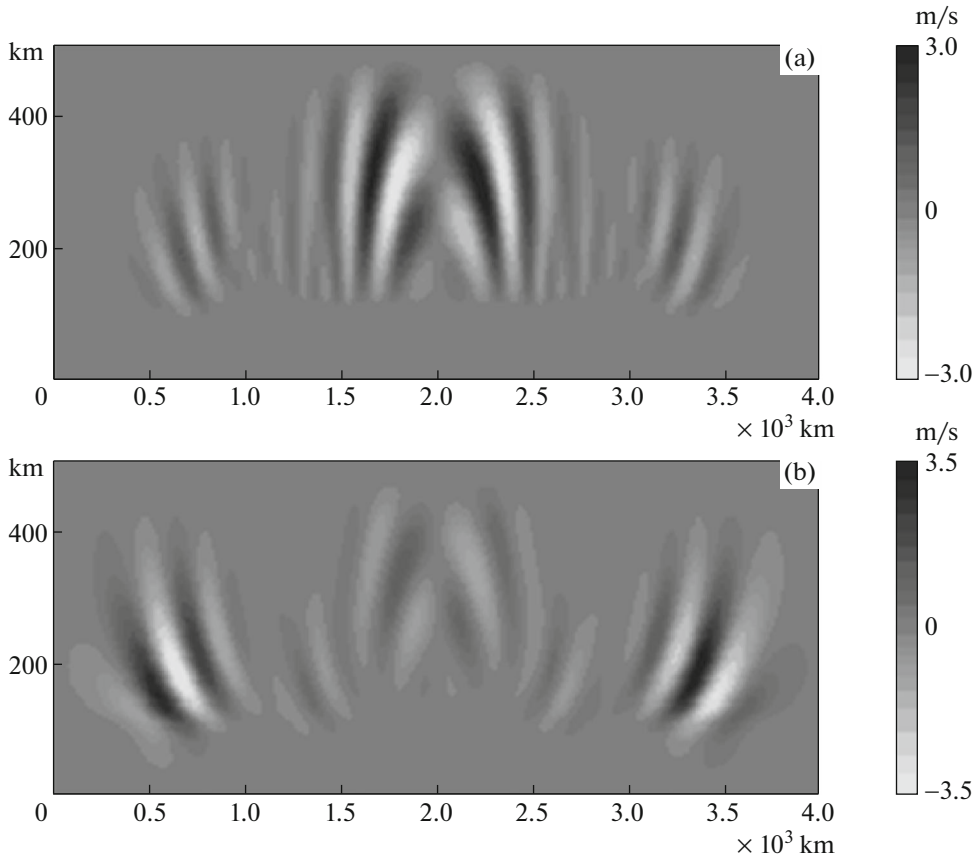

Fig. 1. The spatial distributions of the horizontal velocity, u, of hydrodynamic particles at the time point $t = 5500$ s after the onset of a disturbance from (a) pulse and (b) long-period sources, which produced disturbances in the upper atmosphere that are approximately equal in amplitude.

of a tsunami from its origination in mid-ocean to its arrival at a shore.

3. NUMERICAL SIMULATION RESULTS

The simulation was carried out with the use of the specially developed software [9] for numerical calculation of the set of equations (1) on the basis of the FCT method [11] on a uniform orthogonal grid with 5-km steps in horizontal coordinates and height and a 0.1-s time step. The horizontal size of the simulation domain was approximately 6000 km (depending on the disturbance source) and the height was 500 km. The time range of the calculations was up to 50 000 s (approximately 14 hr). The AGW generation and propagation were studied numerically for the above-mentioned surface sources and for those of their parameters for which the possibility of the excitation of strong disturbances in the upper atmosphere has been confirmed by observation data. They are earthquakes and explosions with the spatial scale $D_x <$ 100 km, amplitude $w_0 < 10$ m/s, and the period $P < 1$–2 s; large-scale long-period oscillations of the Earth's surface with $D_x < 800$ km, $P = 0$–10 000 s, and the displacement amplitude $h_0 < 1$ m; long-period water surface oscillations (seiches) with the displacement amplitude $h_0 = 0.3$–3 m and the characteristic period $P = 1$–3 h; thermal heating of the surface air layer with the scale $D_x < 100$ km and the amplitude $T_0 = 0.1$–5 K; and tsunamis with the scale $\lambda = 100$–200 km, amplitude of displacement in the mid-ocean $h_0 = 0.01$–1 m, amplitude of displacement on a coast $h_0 = 5$–10 m, and the velocity $v = 200$–300 m/s. Profiles of the background temperature, density, and molecular weight of the real atmosphere taken from the MSIS-90 model for all the fours seasons were used.

The analysis of the results has shown the possibility in principle of AGW generation in the atmosphere by the surface sources under study and for background atmospheric profiles. The following general laws in propagation of a disturbance in the upper atmosphere were ascertained for all of the sources: the formation of a stable pattern of an acoustic disturbance with source-dependent horizontal scales of approximately 100 km and vertical scales of 400 km over the center of a surface source at mesopause altitudes and higher and generation of IGW trains with lengths from two to sev-

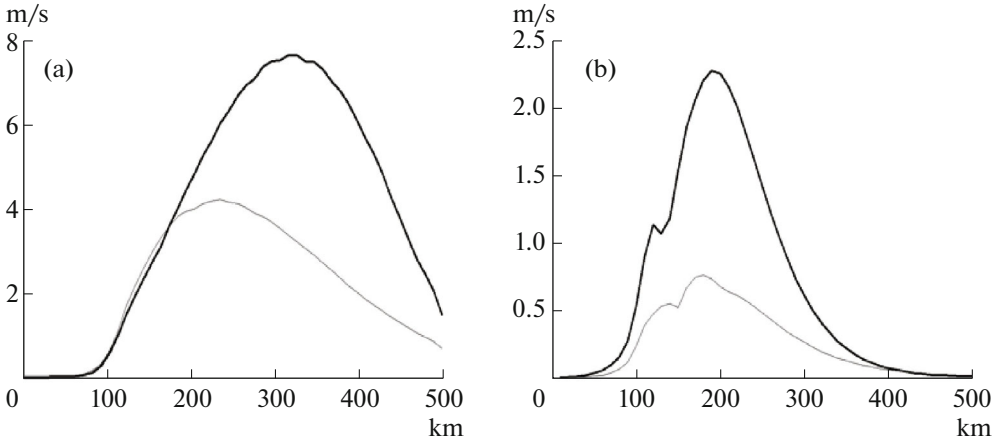

Fig. 2. The comparative dependences of the maximal (a) vertical velocity, w, over the source and (b) horizontal velocity, u, at a distance of 1000 km from the source for a pulse (solid curve) and long-period (dashed curve) sources.

eral tens of wavelengths, which were captured in a waveguide channel at altitudes above the mesopause and horizontally propagated from the source at a downward angle (Figs. 1a and 1b). During further propagation, the period and wavelength of IGWs increased with the distance. The period increased by 120–150 s on average as compared to the gravity wave period over the source epicenter at a distance of 2000 km from the source center.

The waves that were simulated belong to both the acoustic and gravity spectra of AGWs. The periods of acoustic waves (AWs) were approximately 170–290 s, while the periods of IGWs were 750–1500 s. Propagating upward during the first 1000 s after the onset of a disturbance, the period of observed AWs was approximately 170–200 s; the period increased up to 220–290 s after the AWs reached an altitude ceiling of 400–500 km and a stable pattern of the acoustic disturbance was formed over the source. The group velocity of AWs varied from 340 to 600 m/s versus altitude; the IGWs had a velocity in the range 250–310 m/s, which insignificantly increased with the distance. The horizontal wavelengths of IGWs were 250–280 km, while those of AWs were 170–200 km. The maximal amplitudes of the horizontal and vertical AW velocities and temperature disturbances immediately over the source were observed at altitudes of 250–350 km (Fig. 2a). The maxima of the corresponding parameters shifted toward the mesopause (altitudes of 150–200 km) at a horizontal distance of 1000 km from the source, where gravity waves predominated (Fig. 2b). The average amplitudes of the horizontal and vertical velocities and the disturbance temperature at the altitude of peak response exceeded their surface values by 300–400 times. For all source types, the amplitude of the vertical velocity, w, and temperature, T, increased at most by 4000–6000 and 2000–3000 times, respectively, immediately over a source.

Let us now consider features of the disturbances that were observed for different source types.

In the cases of earthquakes and explosions, the disturbance spectrum was concentrated mainly in the acoustic range and the disturbance was located over its source (Fig. 1a). The amplitudes of the vertical velocities of AW particles could attain several hundreds meters per second over the source after explosions. Gravity waves were weakly pronounced and their periods were 750–900 s.

For long-period oscillations of the Earth's surface, the maximum possible amplitudes of the horizontal and vertical particle velocities were no more than 20–30 m/s for AWs and 10–30 m/s for IGWs. A disturbance was mainly presented by gravity waves with the periods $P > 1000$ s, which propagated to several thousands of kilometers without significant attenuation (Fig. 1b). The comparative analysis showed that the amplitudes of IGWs that were observed in a numerical experiment are higher in the case of a long-period source than of a short-period source. Thus, the simulation data allows us to ascertain the approximate parameters of a disturbance that is induced by long-term oscillations of the Earth's surface during an earthquake preparation period. In addition, the numerical calculations allow us to assert that reliable signals of an earthquake can be detected on the basis of the analysis of ionospheric disturbances at large horizontal distances from the source [4].

Let us now consider simulation of seiches. The calculations showed that seiches are capable of generating mainly long-period atmospheric AGWs. (Figs. 3a and 3b). The amplitudes of the horizontal and vertical particle velocities in IGWs that were excited by model sources that corresponded to seiches in Lakes Geneva, Baikal, and Michigan [12], usually did not exceed 1 m/s. IGWs in that case propagated in the form of several successive trains, following one

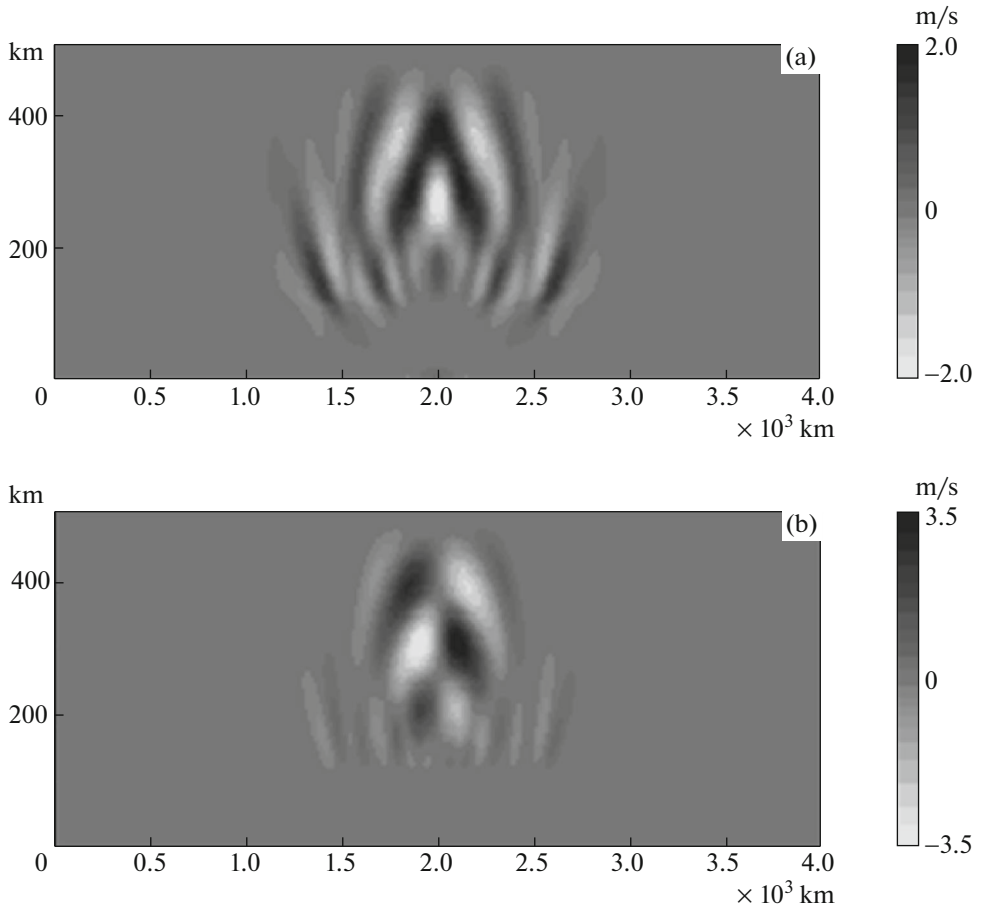

Fig. 3. The spatial distributions of the (a) horizontal, u, and (b) vertical velocity, w, of hydrodynamic particles at $t = 5600$ s for a source that simulated seiches with an amplitude $h_0 = 2$ m, period $P = 10000$ s, and spatial scale $D_x = 300$ km.

another from a source with a lag of 1.5–2 h. The horizontal phase velocity of IGWs was within the 280–300 m/s limits, the period of IGWs was $P \sim 900$–1500 s, and the wavelength $\lambda \sim 320$–450 km.

The IGW amplitudes were quite high (u, $w \sim 30$–50 m/s) in a disturbance produced by a temperature source, as well as their spatial sizes, while AWs were weakly pronounced (Fig. 4a). The amplitudes of the horizontal and vertical particle velocities, u and w, and the temperature, T, were the highest in the disturbance from the temperature source as compared to responses to other disturbance sources under study (Fig. 4b). The comparative analysis showed that a temperature source with the amplitude $T_m = 0.25$ K and long-period oscillations of the Earth's surface with a surface displacement amplitude of approximately tens meters and a period of approximately 1000 s generate IGWs with approximately equal amplitudes.

The simulation of disturbances in the upper atmosphere induced by a tsunami was described in [15], where the authors considered the ionospheric response to the propagation of the tsunami that was induced by the 2011 Tohoku earthquake in detail. In this work, we consider a more complex source to describe the propagation of a tsunami (see the previous section) and wider ranges of variations in the parameters ν, h_0, and λ; however, the general conclusions in [15] were confirmed. These are: the propagation of a tsunami is accompanied by excitation of AGWs in the upper atmosphere; a part of them are ahead of the tsunami, i.e., form a precursor (Fig. 5). During propagation in mid-ocean, the atmospheric response was a disturbance mainly at altitudes of 100–300 km. The wavelengths of the IGWs that led the tsunami were 140–180 km with periods from 100 to 150 s. The train length was approximately 500–1000 km, i.e., 3–5 wavelengths. In addition to the calculations in [15], it was shown that tsunami propagation on the shelf, where the tsunami amplitude sharply increases, sometimes up to 30–40 m, significantly contributes to the final disturbance. These results allow us to state that the amplitudes of the horizontal and vertical velocities of AGWs attain 40–60 m/s at altitudes of the peak response of the atmosphere of 200–250 km. The temperature amplitudes we calculated did not exceed 10–12 K.

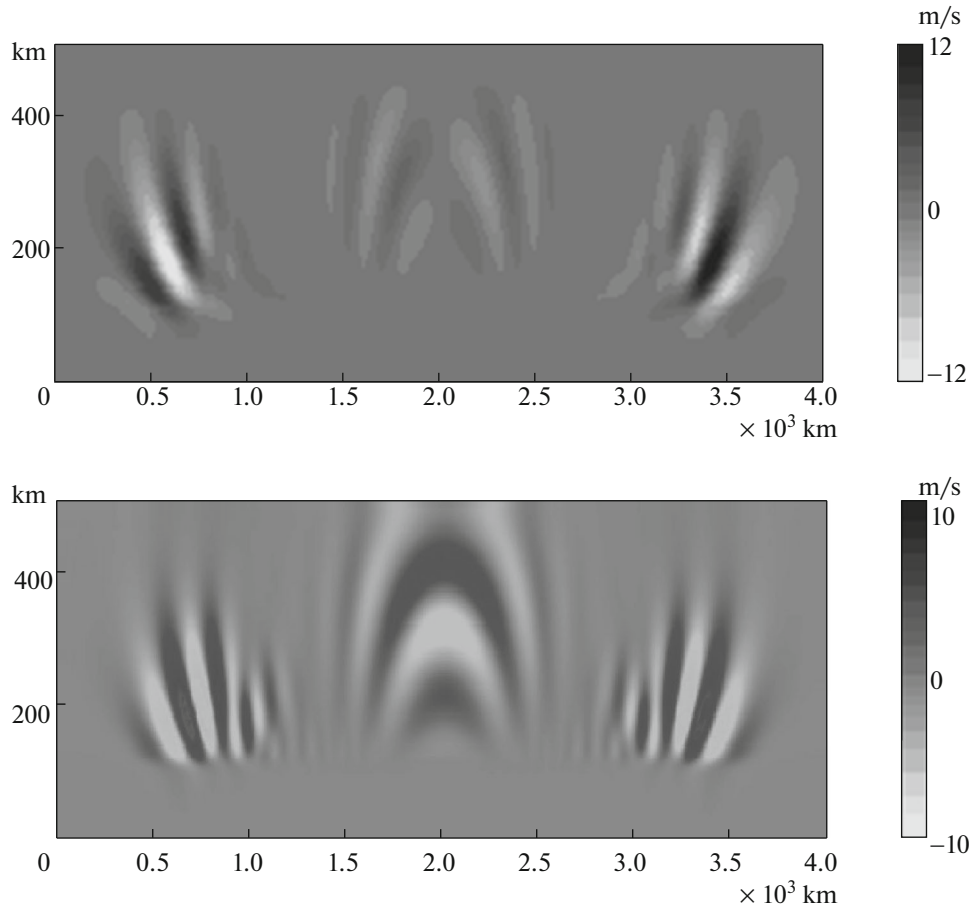

Fig. 4. The spatial distribution of the (a) horizontal velocity, u, and (b) temperature, T, of a disturbance at $t = 6000$ s for a temperature source with an amplitude of 1 K, spatial scale $D_x = 20$ km, and period $P = 3000$ s.

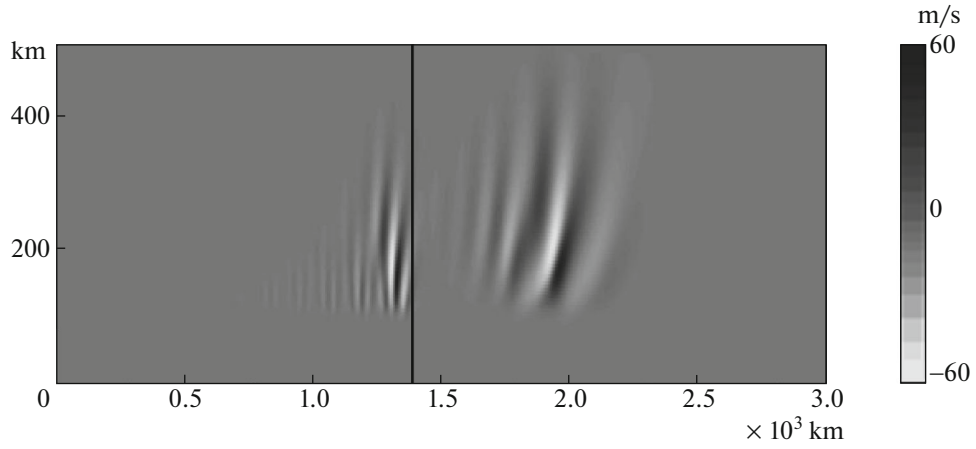

Fig. 5. The spatial distribution of the vertical velocity component, w, of air particles 7 hr after tsunami origination. The tsunami position is marked by the vertical line.

Finally, let us note that our results were compared with the results of experimental and theoretical works in the cases where similar studies were carried out. In general, quite good agreement was noted between parameters of ionospheric disturbances that were observed after large earthquakes [6], chemical and nuclear explosions [6], and tsunami propagation [3, 16] and the numerical calculation results for the

responses of the upper atmosphere to corresponding model sources.

ACKNOWLEDGMENTS

This work was financially supported by the Russian Science Foundation (grant no. 14-17-00637).

REFERENCES

1. E. Calais and J. B. Minster, Phys. Earth Planet. Inter. **105**, 167 (1998).
2. E. M. Lin'kov, L. N. Petrova, and K. S. Osipov, Trans. (Dokl.) USSR Acad. Sci. Earth Sci. Sect. **313**, 76 (1992).
3. J. J. Makela, P. Lognonne, H. Hebert, et al., Geophys. Res. Lett. **38**, L00G02 (2011).
4. V. A. Liperovskii, O. A. Pokhotelov, and S. L. Shalimov, *Ionospheric Precursors of Earthquakes* (Moscow, 1992) [in Russian].
5. S. H. Francis, J. Atmos. Terr. Phys. **37**, 1011 (1975).
6. E. S. Andreeva, M. B. Gokhberg, V. E. Kunitsyn, et al., Cosmic Res. **39**, 10 (2001).
7. E. L. Afraimovich, N. P. Perevalova, A. V. Plotnokov, et al., Ann. Geophys. **19**, 395 (2001).
8. G. I. Grigor'ev, Radiophys. Quantum Electron. **42**, 1 (1999).
9. R. R. Akhmedov and V. E. Kunitsyn, Geomagn. Aeron. (Engl. Transl.) **44**, 95 (2004).
10. M. Pitteway and C. Hines, Can. J. Phys. **41**, 1935 (1963).
11. E. S. Oran and J. P. Boris, *Numerical Simulation of Reactive Flow* (Elsevier, New York, 1987; Mir, Moscow, 1990).
12. *McGraw-Hill Encyclopedia of Science & Technology* (McGraw-Hill, 2003).
13. P. Sauli and J. Boska, J. Atmos. Sol.-Terr. Phys. **63**, 945 (2001).
14. B. V. Levin and M. A. Nosov, *Tsunami Physics* (Moscow, 2005) [in Russian].
15. V. E. Kunitsyn and A. M. Vorontsov, Moscow Univ. Phys. Bull. **69**, 263 (2014). doi doi 10.3103/S0027134914030096
16. J. Artru, V. Ducic, H. Kanamori, et al., Geophys. J. Int. **160**, 840 (2005).

Translated by O. Ponomareva